JOURNAL OF MATERIALS SCIENCE 25 (1990) 4401–4404

RMS matrix strains in transformation toughened alumina

K. R. WILFINGER
Lawrence Livermore National Laboratory, PO Box 808, L-369, University of California, Livermore, CA 94550, USA

W. R. CANNON
Center for Ceramic Research, Rutgers University, Busch Campus, PO Box 909, Piscataway, New Jersey 08855-0909, USA

T. TSAKALAKOS
Department of Material Science, Rutgers University, Busch Campus, PO Box 909, Piscataway, New Jersey 08855-0909, USA

The Warren Averbach technique was used to determine the RMS strain profile in the Al_2O_3 matrix surrounding ZrO_2 particles in zirconia toughened alumina. The X-ray domain size was found to be ~100 nm in all but the most severely microcracked sample. The RMS strain, averaged over all domains, decreased nearly linearly from the edge of the domain (presumably from the ZrO_2 particle), except when microcracking was detected and then the RMS strain level was reduced near the surface of the domain. The maximum RMS strain level increased with increasing ZrO_2 particle size up to the point where microcracking occurred then decreased. The results were explained by noting that the maximum RMS strain was directly related to the monoclinic content of the sample.

1. Introduction

The strengthening of transformation toughened alumina depends largely on the $ZrO_{2(tetragonal)} \rightleftarrows ZrO_{2(monoclinic)}$ phase transformation. Stresses in the Al_2O_3 matrix surrounding the ZrO_2 particles and within the particle itself can affect the transformation in several ways. Internal stresses may promote nucleation [1], matrix strain energy associated with the transformation may be partially responsible for the particle size dependence of transformation [2] and interactive stresses between transforming particles may promote transformation [3, 4].

Stresses surrounding ZrO_2 particles in transformation toughened alumina have three possible sources: (1) the thermal expansion mismatch between Al_2O_3 and ZrO_2, (2) stress due to the volume dilation and shear associated with the transformation and (3) short range stresses due to the twin-matrix interface. The short range stresses have been discussed by Evans *et al.* [5]. The former two stresses have been treated theoretically and experimentally only in a very limited manner. The non-vanishing strain tensor for the unconstrained transformation has been given by Chen and Chiao [6] and the strain tensor for the unconstrained thermal expansion mismatch is given by Schmauder [7]. Calculations for the elastic strains both inside and outside octrahedrally shaped particles have been made [8] but remain unpublished.

Kriven [9] examined the thermal expansion mismatch strains using TEM. He demonstrated that the strains are tensile and maximum along a line parallel to the *c*-axis of the tetragonal particle regardless of orientation of the matrix. Strains were still detectable at a distance approximately equal to the diameter of the particle. The measurements were, however, on a foil only twice the diameter of the particle thickness and it was necessary to anneal the foil prior to TEM examination. Furthermore, quantitative values for the strain distribution were not obtained.

In this study the Warren-Averbach technique [10] was used to determine the RMS strain distribution around ZrO_2 particles in Al_2O_3–10% ZrO_2 bulk samples. The Warren-Averbach approach separates broadening due to X-ray domain size and microstrains. Polycrystalline Al_2O_3 was used as a standard to determine instrumental broadening. This eliminates thermal expansion anisotropy strains in the Al_2O_3 leaving only strains due to the ZrO_2 particles themselves. It was then possible to measure the RMS strain distribution in several samples of varying ZrO_2 particle size to determine the size effect.

2. Experimental procedure

Samples were prepared by sintering Al_2O_3–ZrO_2 compacts. Submicron ZrO_2 powder for the composite was obtained by vibro-energy milling commercial zirconia (SC30 ZrO_2, Magnesium Elektron, Flemington, New Jersey.) in water, followed by Stokes' settling under the influence of gravity and using a continuous centrifuge. The distributions were measured using a light scattering spectrometer. (PCS 4700 Light scattering spectrometer, Malvern Instruments, Waltham, Massachusetts.) Particle size range above which no particles were detected was 0.71–0.86, 0.59–0.71 and 0.48–0.58

0022–2461/90 $03.00 + .12

micrometre, respectively for Samples *F*, *J* and *G*. In comparison the as-received powder had an uppersize of $\sim 20\,\mu m$ (Sample *C*) and powder not subjected to the continuous centrifuge but milled had an upper size of $1.4\,\mu m$ (Sample *V*).

The various classes of zirconia were incorporated at a constant 10 volume per cent in alumina (A16SG Al_2O_3, Aluminium Company of America, Pittsburgh, Pennsylvania.) by pressure casting of aqueous slips containing 50 v/o total solids with ammonium-polyacrylate (Darvan 821A, R. T. Vanderbilt, Nowalk, CT.) as a dispersant. Disc shaped samples approximately 2.5 cm in diameter by 0.5 cm thick were cast. The green samples were carefully flattened on one side using SiC paper in order that X-ray measurements may be made on a flat unground surface after firing. Debris from grinding was removed with a sable brush and the samples were fired for one hour at 1600° C. The fraction of tetragonal zirconia in each sample was calculated from X-ray integrated intensity data using the method of Porter and Heuer [12].

Samples were polished and thermally etched and examined under SEM. Quantitative microscopy was applied to sample *F* to determine the size distributions of ZrO_2 particles. Results presented in another paper [4] showed that the ZrO_2 particle size distribution changed very little during sintering (measured on Sample *F*) but that $\sim 10\%$ of the particles touched each other. Both dynamic light scattering and quantitative microscopy were unable to detect particles much above the upper size limit specified above. For instance, in sample *F* using image analysis on a polished surface no particles were detected with an equivalent spherical diameter greater than $1.1\,\mu m$.

Elastic moduli of the various sintered samples were measured using an elastic through-transmission technique described by Bhardwaj [11].

The previously prepared faces of the sintered samples were examined using the Warren-Averbach technique [9] for measuring apparent RMS strain by X-ray line broadening. A theta–theta diffractometer (Kristalloflex D500T, Siemens.) was employed, step scanning over the ranges 40.5 to 45.5 and 92.5 to 97.5 degrees 2-theta, measuring for 10 seconds every 0.02 degrees. The peaks of interest were the 113 and 226 reflections for corundum, occurring at 2-theta angles of 43.4 and 95.3 degrees respectively (CuKα radiation). The raw intensity data in counts per second was processed by computer using a Fourier transformation program. The Fourier coefficients produced were then analysed, in order to determine the average size of the X-ray diffracting domain and the average RMS strain distribution in the matrix of each sample. Polycrystalline Al_2O_3 was used to subtract out the instrumental broadening.

3. Results and Discussion

3.1. Elastic modulus and monoclinic fraction

The average elastic moduli and fraction of monoclinic zirconia at room temperature in the samples studied are given in Table I. The room temperature monoclinic fraction in the composites increased with increasing zirconia particle size from approximately 2 per cent for the body with the finest powder to 100 per cent for the body with as-received material. The elastic moduli of bodies *F*, *J* and *G*, containing only submicron zirconia, were all approximately 350 GPa, which is very near the weighted average for alumina–10 v/o zirconia composite. This is a good indication that the samples were of similar quality and contained few, if any, microcracks which could reduce their effective elastic moduli. It is logical to conclude that the reductions in modulus observed in materials containing the coarse tail resulted from microcracking due to stresses associated with the tetragonal to monoclinic transformation. Flexure strength measurements on samples of the same composition (not covered in this discussion) confirmed the degradation in mechanical properties implied by the elastic modulus results.

TABLE I Elastic moduli of sintered alumina–zirconia composites

Sample	E ($\times 10^6$ p.s.i.)	Monoclinic content (%)
Al_2O_3	54.0	
ZrO_2 [15]	27	
Weighted average	51.3	
C (as-received)	30.0	100%
V (< 1.4 micrometres)	47.8	62%
F (< 0.86 micrometres)	50.9	10%
J (< 0.71 micrometres)	50.2	5.8%
G (< 0.58 micrometres)	50.5	2%
B (mixed 90% *V* and 10% *F*)	49.8	35%

3.2. Alumina X-ray domain size

The Warren-Averbach technique deconvolutes the contributions to X-ray line broadening due to domain size effects from those due to non-uniform strain. This is possible because the degree of broadening due to domain size effects is independent of the order of the reflection, while that due to strain is not. Figure 1 shows a typical plot of Fourier coefficient against depth into the X-ray domain. The shape of the curve shows several classical features. The non-linear portion of the curve near $L = 0$ is called the hook and is related to inaccuracies in determining the shape of the tail of the X-ray peak. All curves extrapolated directly to one at $L = 0$ without normalization as expected from the derivation but not usually found experimentally. Extrapolation of the linear part of the curve to $A_s = 0$ yields the average domain diameter. The average X-ray domain diameters measured for the alumina bodies containing zirconia were all approximately 0.1 micrometre, with one exception. Body *C*, containing coarse ZrO_2 particles had domains too large to measure because they fell outside the range that leads to domain size broadening in the X-ray curves.

The physical significance of the $0.1\,\mu m$ X-ray domain diameter in the Al_2O_3 matrix is difficult to determine. This diameter is much smaller than the grain size, which is about $1\,\mu m$, and generally, subgrain boundaries are not present in fine grained transformation toughened alumina [13]. However, the presence of dislocations or twins in the Al_2O_3 grain

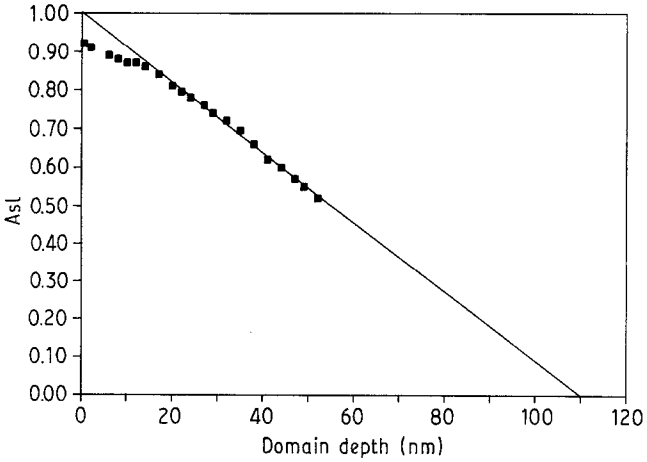

Figure 1 Fourier coefficients due to strain broadening against depth into domain.

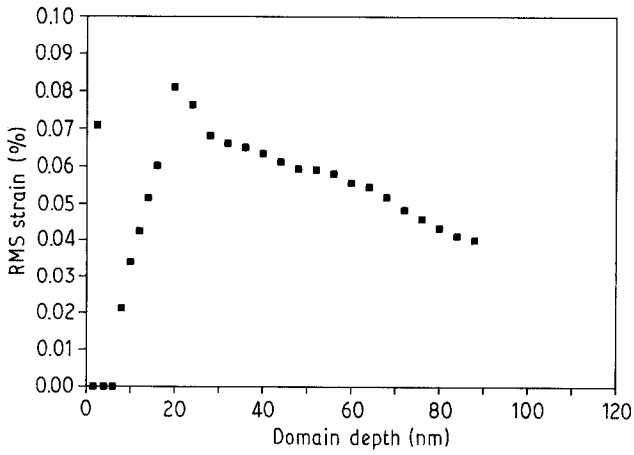

Figure 3 RMS strain against depth into domain for sample C which is microcracked.

could reduce the effective size of the X-ray domain and account for the measured domain diameter.

3.3. Apparent RMS strain determination

Fig. 2 shows RMS strain results as a function of distance into the domain for bodies containing sub-micron ZrO_2 (samples *F*, *J*, and *G*). In general, the average RMS strain measured in the alumina matrices of the samples under study was greatest near the edges of the domain, declining roughly linearly to half its peak within 200 nanometres (0.02 micrometres). This was a much faster decline than expected. The RMS strain for sample *C* ($< 20\,\mu m$ ZrO_2), Fig. 3 declined more slowly, reaching half its peak within 700 nanometres (0.07 micrometres).

The shape of the curve for samples *V* and *C* was somewhat different. The curve for sample *C* is shown in Fig. 3. The stress is not maximum at the surface of the domain but it appears that the stress is relieved near the surface which may be due to microcracking around the ZrO_2 particles. The stress profile of sample *G* ($0.6\,\mu m$), Fig. 2 also is a bit anomalous in that it decreases as the others but rises again. This rise may result from the nearer proximity of ZrO_2 particles in Sample *G* (since at a constant volume per cent finer particles are closer to one another) where neighbouring stress fields overlap or it may be attributed to background effects at the low intensity.

The maximum RMS strains for all of the samples are plotted in Fig. 4 as a function of the upper end of the zirconia size range before sintering. The elastic moduli of the various samples is also shown in Fig. 4. It is apparent that the maximum RMS strain increases as the zirconia particle size increases, up to the point where significant microcracking begins. After that, the microcracks act to relieve stresses near the surface of the domain and lower the maximum RMS strain.

It is well known from elasticity theory that the magnitude of the stresses at the particle surface are independent of particle size and so it is surprising that the maximum stress would vary with particle size. An alternative explanation is that the monoclinic content increased with increasing upper size of the particles, the reason apparently being that increasingly larger number of particles exceed the critical size, d_c. The maximum RMS strains associated with the three samples containing sub-micron zirconia are replotted as a function of monoclinic content in Fig. 5. It is apparent that, in the absence of microcracking, there is a definite relationship between the fraction of zirconia transformed and the RMS strain measured.

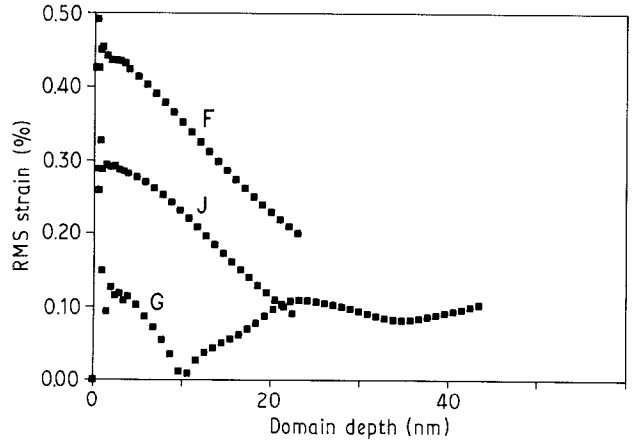

Figure 2 RMS strain as a function of domain depth for samples, F, J and G.

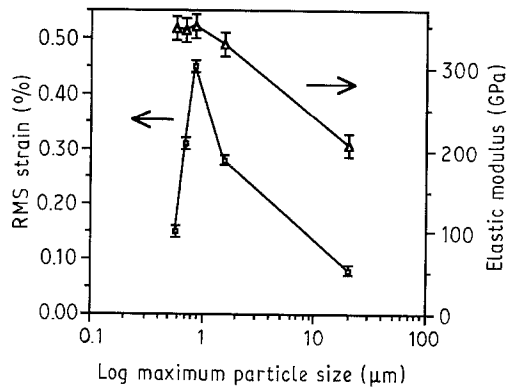

Figure 4 Maximum RMS strain and elastic modulus as a function of upper end of particle size range.

* #X-86-N hot-stage, MRC Industries,
† #12215/0, Philips Instruments, Mahwah, NJ.

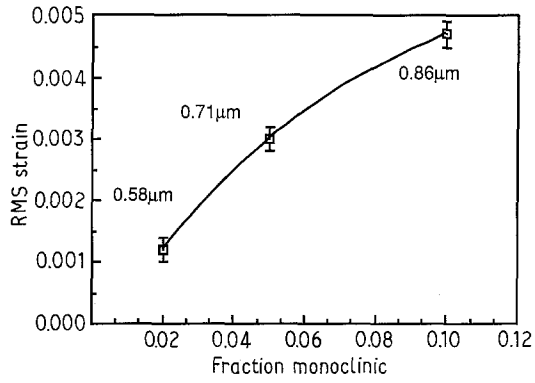

Figure 5 Maximum RMS strain against fraction of monoclinic.

3.4. Calculation of predicted average RMS strain in domain

A general explanation for Fig. 5 is that the Warren-Averbach technique averages RMS strains over all domains and so as the monoclinic fraction increases, so does the magnitude of the average RMS strain. According to this point of view the RMS strain may be considered to be an average of three types of domains: those adjacent to monoclinic particles, those adjacent to tetragonal particles and those not adjacent to ZrO_2 particles. For simplicity we will consider the RMS strain in the latter category to be zero. The average RMS strain is thus given as

$$\varepsilon(\text{RMS}) = \{\alpha X_m[\varepsilon(3\,1\,1, \text{monoclinic})]^2 + \alpha(1 - X_m) \times [\varepsilon(3\,1\,1, \text{tetragonal})]^2 + (1 - \alpha)[\varepsilon(\text{others})]^2\}^{1/2} \quad (1)$$

where α = Fraction of matrix domains adjacent to zirconia particles, X_m = Fraction of zirconia particles converted to monoclinic, $\varepsilon(3\,1\,1, \text{monoclinic})$ = Maximum dilatational strain in domains surrounding monoclinic ZrO_2 particles measured along the $\langle 3\,1\,1\rangle$ direction of the Al_2O_3 lattice. $\varepsilon(3\,1\,1, \text{tetragonal})$ = Maximum dilatational strain in domains surrounding tetragonal ZrO_2 particles measured along the $\langle 3\,1\,1\rangle$ direction of the Al_2O_3 lattice.

This equation can be rearranged as follows

$$\varepsilon(\text{RMS}) = (AX_m + B)^{1/2} \quad (2)$$

where $A = \alpha[\varepsilon(3\,1\,1, \text{monoclinic})]^2 - \alpha[\varepsilon(3\,1\,1, \text{tetragonal})]^2$, $B = \alpha[\varepsilon(3\,1\,1, \text{tetragonal})]^2 + (1 - \alpha) \times [\varepsilon(\text{others})]^2$.

The data points fit exactly if $A = 2.57 \times 10^{-4}$ and $B = -3.76 \times 10^{-6}$ and the curve is shown in Fig. 4. B, however, cannot be negative but since both $[\varepsilon(3\,1\,1, \text{tetragonal})]^2$ and $[\varepsilon(\text{others})]^2$ are very small the value is difficult to determine accurately. The strain $[\varepsilon(3\,1\,1, \text{monoclinic})]$ may be calculated from A if α is known. For a spherical ZrO_2 particle surrounded by domains 0.1 μm thick $\alpha \approx 0.17$ and if $\alpha[\varepsilon(3\,1\,1, \text{tetragonal})]^2$ is neglected, $[\varepsilon(3\,1\,1, \text{monoclinic})] = 0.04$ which is the right order of magnitude for the dilatational strain of ZrO_2 during the $t \rightarrow m$ transformation.

4. Conclusion

RMS strains resulting from ZrO_2 particles in an Al_2O_3 matrix appear to be directly related to the monoclinic content. Results are consistent with a model in which strains are averaged around monoclinic and tetragonal particles and so the Al_2O_3 matrix RMS strain appears to be dominated by the RMS strain surrounding monoclinic particles.

Acknowledgement

This work was supported by the Center for Ceramic Research at Rutgers University.

References

1. A. H. HEUER and M. RUHLE, *Acta Metall.* **33** (1985) 761.
2. F. F. LANGE, *J. Mater. Sci.* **17** (1982) 225.
3. K. R. WILFINGER and W. R. CANNON, *J. Am. Ceram. Soc.* **72** (1989) 1256.
4. I-WIE CHEN and P. E. REYES-MOREL, in "Mater. Res. Soc. Symp. Proceedings, Vol. 78, *Advanced Structural Ceramics*, edited by P. F. Becher, M. V. Swain, and S. Somiya, (Materials Research Society, Pittsburgh, 1987).
5. A. G. EVANS, N. BURLINGAME, M. DRORY and W. M. KRIVEN, *Acta Metall.* **29** (1981) 447.
6. I.-W CHEN and Y.-H. CHIAO, *Acta Metall.* **13** (1983) 1627.
7. S. SCHMAUDER, W. MADER and M. RUHLE, in "Advances of Ceramics, 12", edited by N. Claussen, M. Ruhle, and A. H. Heuer, (Am. Ceram. Soc. (1984)) p. 251.
8. T. TSAKALAKOS, "Micromechanics and Inhomogeneities", edited by G. J. Wang (Springer-Verlag, New York, 1990) p. 469.
9. W. M. KRIVEN, in "Advances of Ceramics 12", edited by N. Claussen, M. Ruhle, and A. H. Heuer, (Am. Ceram. Soc. 1984) p. 64.
10. B. E. WARREN and B. L. AVERBACH, *J. Appl. Phys.* **21** (1950) 595–99.
11. M. C. BHARDWAJ, Company Publication, Ultran Laboratories Inc., State College, PA (1985).
12. D. L. PORTER and A. H. HEUER, *J. Am. Ceram. Soc.* **62** (1979) 298.
13. M. RUHLE, private communications.

Received 9 December 1988
and accepted on 31 May 1989